J. Fluid Mech. (1995), *vol.* 292, *pp.* 305–323

Stability of two-dimensional convection in a fluid-saturated porous medium

By M. DE LA TORRE JUÁREZ[1] AND F. H. BUSSE[2]

[1]ETSI Aeronáuticos, Pza. Cardenal Cisneros 3, 28040 Madrid, Spain

[2]Institut für Theoretische Physik IV, Universität Bayreuth, 95440 Bayreuth, Germany

(Received 20 June 1994 and in revised form 9 February 1995)

The range of existence and the stability of spatially periodic solutions has been studied for steady and oscillatory two-dimensional convection in a fluid-saturated porous medium. We have analysed the limit where viscous effects are dominant and Darcy's law can be applied. A Galerkin method has been used to obtain the steady and the centrosymmetric oscillatory solutions that appear in nonlinear convection at Rayleigh numbers up to 20 times the critical value. Their stability boundaries to arbitrary infinitesimal perturbations have been obtained. Above a given Rayleigh number stable oscillatory solutions are possible at wavenumbers close to the critical values. The stability of this oscillatory state with respect to infinitesimal perturbations of any wavenumber has also been studied. The resulting temporal dynamics in the different unstable regimes is briefly discussed. We show the existence of 3:1 spatial resonances of the steady roll solutions and the existence of stable centrosymmetric and non-centrosymmetric oscillatory solutions.

1. Introduction

The study of thermal convection in a fluid heated from below has attracted much interest as one of the simplest hydrodynamical systems in which the evolution towards turbulent flows can be investigated. The transition to turbulence starts from a simple steady state that evolves through subsequent transitions (Krishnamurti 1970*a*,*b*; Busse 1978). Oscillatory convection seems to play an important role in this evolution to complex temporal behaviour. Experimental studies of the transition to complex flows have been carried out in nearly square boxes, where the spatial structure of the flow is strongly constrained (Ahlers & Behringer 1978; Bergé & Dubois 1979; Maurer & Libchaber 1979; Gollub & Benson 1980). A main motivation for the present analysis has been an improved understanding of the dynamics of convection in narrow horizontal fluid-filled channels heated from below. The analogy between two-dimensional convection in a porous medium and convection in a Hele-Shaw cell has often been emphasized in the literature (Wooding 1960; Kvernvold 1979) and will be exploited by the present analysis. Unfortunately the idealized boundary condition of vanishing heat conductivity of the side walls in the Hele-Shaw configuration is difficult to realize in laboratory experiments. Observations such as those of Koster & Müller (1984) thus agree only qualitatively with the theoretical predictions. Nevertheless, the basic system of equations to be studied in this paper represents the simplest case of a realistic fluid dynamical system in which the evolution from simple to complex flows can be investigated through three

or four bifurcations. The results of the analysis are thus meant to serve as a guide for more detailed investigations required for quantitative comparisons with experiments.

The stability analysis of nonlinear steady convection in an Hele-Shaw cell was carried out by Kvernvold (1979). He obtained stability boundaries with respect to infinitesimal wavenumber-changing perturbations of the stationary solutions. He showed that for each value of the Rayleigh number Ra there is a band of stable wavenumbers α. But, except for low values Ra, the instabilities occurring at each end of the wavenumber band are different. For a limited region above the critical Rayleigh number steady roll solutions become unstable at both ends of the wavenumber band via the Eckhaus instability. Above a Rayleigh number of the order of $Ra = 8Ra_c$ solutions with a wavenumber equal to the critical value α_c and smaller are unstable to oscillatory convection. The critical Rayleigh number for the onset of this oscillatory instability depends strongly on the value of α. At the other end of the stable wavenumber band, Kvernvold obtained an Eckhaus instability for all Rayleigh numbers up to 20 times the critical. A similar study has been carried out for convection in a porous medium in a two-dimensional (Caltagirone 1975) and in a three-dimensional geometry (Strauss 1974). The results in the two-dimensional case show a behaviour similar to that in the Hele-Shaw case, but yield an onset for oscillatory convection slightly above $10Ra_c$. This value differs from the one obtained by Kvernvold (1979), but it is closer to the one obtained in later works and in ours. The study of the three-dimensional case shows that at $Ra = 9.6Ra_c$ cross-roll convection sets in for $\alpha = \alpha_c$, indicating that three-dimensional effects become important before oscillatory convection occurs.

Detailed numerical analyses of the onset of oscillatory convection and the transition to chaos have been carried out for wavenumbers close to the critical value either in a finite two-dimensional container (Frick & Müller 1983; Steen & Aidun 1988; Caltagirone & Fabrie 1989; Graham, Müller & Steen 1992), or in a cubic box (Kimura, Schubert & Strauss 1986). Steen & Aidun confirmed the results of Caltagirone for the onset of two-dimensional oscillatory convection and obtained the critical value $Ra = 391$ at $\alpha = \alpha_c$. In the present study, we review the stability analysis of steady convection with respect to infinitesimal two-dimensional perturbations of arbitrary wavenumber. We have analysed the oscillatory solutions of finite amplitude that appear at wavenumbers close to the critical one and have studied their stability as a function of the wavenumber for different Rayleigh numbers. The regimes where the solutions become unstable have also been studied via numerical simulations in order to understand the dynamics of the unstable flow.

2. Mathematical description of the problem

We consider a fluid-saturated porous medium heated from below and cooled at its upper boundary. The porous layer is of infinite extent in the horizontal direction and has the height h. In a fluid-saturated porous medium of small pore size with dominant viscosity, inertial effects can be neglected. This approximation is known as Darcy's law. If we nondimensionalize the equations using h^2/K, as the time scale, the thickness h of the fluid layer as the length scale and ΔT as temperature scale, we obtain in the Boussinesq approximation (see for instance Strauss 1974) for the

equations of motion and the energy equation:

$$\boldsymbol{u}(x,z,t) = -\nabla P + Ra\theta\boldsymbol{k}, \tag{2.1a}$$

$$\nabla\cdot\boldsymbol{u} = 0, \tag{2.1b}$$

$$\partial_t\theta(x,z,t) + \boldsymbol{u}(x,z,t)\cdot\nabla\theta(x,z,t) = \boldsymbol{u}(x,z,t)\cdot\boldsymbol{k} + \nabla^2\theta(x,z,t), \tag{2.1c}$$

where $\boldsymbol{u}(x,z,t)$ is the velocity, $\theta(x,z,t)$ is the deviation of the temperature from the state of pure conduction with the constant thermal diffusivity K; $Ra = \gamma g h k \Delta T/\nu K$ is the Rayleigh number with the coefficient of the thermal expansion γ, the permeability of the porous medium k and the kinematic viscosity ν; P is the dynamic pressure. Since the temperatures at the boundaries are fixed with the difference δT the boundary conditions are $\theta = w \equiv \boldsymbol{k}\cdot\boldsymbol{u} = 0$ at $z = \pm\frac{1}{2}$. The boundary conditions in the horizontal direction are taken to be periodic. Since we are interested in two-dimensional motions, we write the velocity as the curl of a stream function $\psi(x,z,t)\boldsymbol{j}$. We thus obtain

$$\nabla^2\psi = Ra\partial_x\theta, \tag{2.2a}$$

$$\partial_t\theta + J(\psi,\theta) = \partial_x\psi + \nabla^2\theta. \tag{2.2b}$$

The first equation is linear and can be solved directly to yield ψ as a function of θ. The energy equation (2.2*b*) has a nonlinear term given by the Jacobian of ψ and θ. We use a Galerkin method to solve the equations. For that purpose the solution is written as an expansion in the eigenfunctions of the linear stability problem, corresponding to trigonometrical functions (see for instance Wooding 1960),

$$\theta(x,z,t) = \sum_{m=1}^{\infty}\sum_{l=-\infty}^{\infty}\sum_{n=-\infty}^{\infty} b_{mln}\mathrm{e}^{\mathrm{i}l\alpha x + \mathrm{j}n\omega t}\sin m\pi(z+\tfrac{1}{2}).$$

The stream function ψ is given as a solution of (2.2*a*):

$$\psi(x,z,t) = -Ra\sum_{m=1}^{\infty}\sum_{l=-\infty}^{\infty}\sum_{n=-\infty}^{\infty}\frac{\mathrm{i}l\alpha}{l^2\alpha^2+m^2\pi^2} b_{mln}\mathrm{e}^{\mathrm{i}l\alpha x+\mathrm{j}n\omega t}\sin m\pi(z+\tfrac{1}{2}).$$

The amplitudes of the Fourier modes b_{mln} are quaternions (complex numbers on a $C\wedge C$ complex space) and i and j are the imaginary units. Eigenfunctions periodic in time have been introduced in order to account for the possibility of stationary solutions that are oscillatory in time. With this expansion our equations of motion become a set of infinite algebraic equations with the complex amplitudes b_{mln} and the frequency ω as the unknowns. For the steady solutions, ω vanishes, but for oscillatory states we have one equation fewer than unknowns. We solve the problem by taking advantage of the translation invariance in time. We thus fix the phase of a particular component, say b_{111}, at $t = 0$ by requiring $\mathrm{Im}(b_{111}) = 0$. The resulting set of algebraic equations is then solved numerically with a root-finding Newton–Raphson algorithm.

In our numerical scheme, the Fourier series must be truncated at some highest mode N. This determines the spatial resolution of our calculations, giving the maximum wavenumber that can be resolved. On the other side, α corresponds to the minimum wavenumber we can resolve (i.e. the maximum size of the numerical box for which periodic boundary conditions apply). The condition $m+l < N$ was used as truncation scheme in order to reduce the computing time and memory requirements without losing significant information (for a discussion see for instance Veronis 1966).

The symmetry properties of the equations can be used to reduce the numerical effort. As the temperature deviation θ is invariant under reflections in the horizontal direction, we expect $b_{mln} = b_{m-ln}$ and, since θ is a real function, the condition

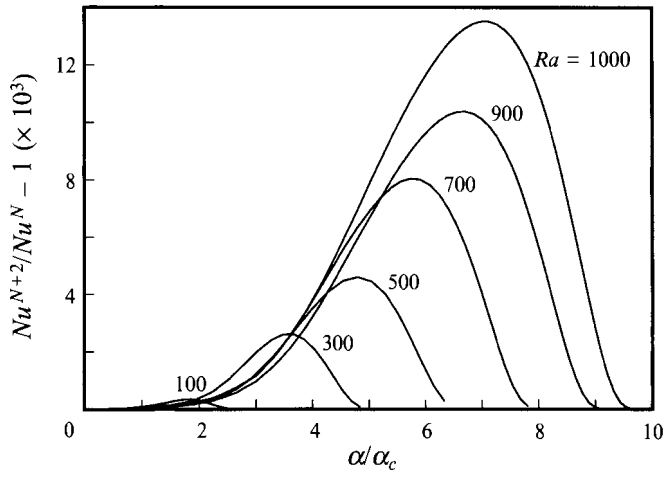

FIGURE 1. Relative error in the Nusselt number depending on the truncation parameter $(m+l<N)$ as a function of the wavenumber α/α_c for different values of the Rayleigh number.

$b_{mln} = b^{+}_{m-ln} = b^{*}_{ml-n}$ must be satisfied. Here the plus stands for complex conjugate in i and the star for complex conjugate in j.

From the linear stability analysis of the pure heat-conducting state one can see (see for instance Wooding 1960) that the first unstable mode corresponds to $m = 1, l = 1, n = 0$. The bifurcating solution is characterized by the property that all coefficients with $l+m =$ odd vanish. We therefore call this solution centrosymmetric or the even rolls. Because of the nature of the nonlinear coupling term, the $m+l =$ odd modes can appear only via a bifurcation from the even rolls. The $l+m =$ even symmetry has also been used to reduce the numerical effort needed to obtain the steady solutions.

The criterion for the choice of our truncation parameter N is based on the value of the Nusselt number Nu at the critical wavelength. The Nusselt number is given by the ratio between the total heat transferred and the heat transferred by conduction. Its spatial average at the bottom wall can be written as

$$Nu(t) = \sum_{n>-M}^{n<M} Nu_n e^{jn\omega t} = \sum_{m=1}^{m<N} \sum_{n>-M}^{n<M} m\pi b_{m0n} e^{jn\omega t}.$$

When the Nusselt number obtained for the solution with wavenumber α_c and N modes is equal to the one obtained with $N+2$ modes, with a relative error of 10^{-3}, we have kept N modes, otherwise we have increased N until this condition is fulfilled. In this case the amplitudes of the Fourier modes corresponding to the low-wavenumber modes were typically more than three orders of magnitude bigger than the amplitudes of the high-wavenumber modes.

An estimation of the error obtained with this truncation condition is given in figure 1. We have plotted the differences between the Nusselt number for $N+2$ and N modes for several Rayleigh numbers as a function of the wavenumber α. It is seen that, for a given Rayleigh number, the error increases for wavenumbers in the middle of the band. We shall see in §3 that this effect is due to a steeper temperature gradient at the boundaries for the middle wavelengths. Nevertheless, the regions of interest are close to the two ends of the wavenumber regime such that this increase in the numerical error is irrelevant.

The truncation order M for the temporal modes is chosen independently of the spatial modes. The condition used to determine M is the requirement that the frequency ω has an absolute error of less than 1 when compared with a higher order truncation $M+1$. This has assured a typical relative error of about $\sim 0.5\%$ in ω. With this condition the typical truncation order is $M = 3$.

Once the stationary solutions $\theta_0(x,z,t)$ are obtained, a linear stability analysis can be carried out. We write the perturbed solutions as $\theta(x,z,t) = \theta_0(x,z,t) + \tilde{\theta}(x,z,t)$ and $\psi(x,z,t) = \psi_0(x,z,t) + \tilde{\psi}(x,z,t)$ and linearize the resulting equations for the perturbations to study their complex growth rates $\sigma \equiv \sigma_r + \mathrm{j}\sigma_j$:

$$\tilde{\theta}(x,z,t) = \sum_{m=1}^{\infty}\sum_{l=-\infty}^{\infty}\sum_{n=-\infty}^{\infty} \tilde{b}_{mln} \mathrm{e}^{\{\mathrm{i}[(l+d)\alpha x + (jn\omega+\sigma)t\}} \sin m\pi(z+\tfrac{1}{2})]. \tag{2.3}$$

The parameter d has been introduced to account for the possibility of perturbations with a wavenumber different from that of the stationary solution; d varies between zero and one. Owing to the reflection symmetry in the horizontal direction, we only need to consider values of d between 0 and 0.5. The interval from $d = 0.5$ to $d = 1$ will be its symmetric reflection. If we insert the expression of the perturbations for the temperature in equation (2.2*a*) we obtain for the perturbation of the stream function:

$$\tilde{\psi}(x,z,t) = \sum_{m=1}^{\infty}\sum_{l=-\infty}^{\infty}\sum_{n=-\infty}^{\infty} \frac{-\mathrm{i}Ra(l+d)\alpha \tilde{b}_{mln} \mathrm{e}^{\{\mathrm{i}[(l+d)\alpha x + (jn\omega+\sigma)t\}}}{(l+d)^2\alpha^2 + m^2\pi^2} \sin m\pi(z+\tfrac{1}{2})]. \tag{2.4}$$

Equation (2.2*b*) can be used to obtain the equation for the perturbations, which is linearized to yield

$$\partial_t \tilde{\theta} + J(\tilde{\psi},\theta) + J(\psi,\tilde{\theta}) = \partial_x \tilde{\psi} + \nabla^2 \tilde{\theta}. \tag{2.5}$$

When this equation is written in Fourier space we obtain a set of linear algebraic equations after using relations (2.3) and (2.4). If all eigenvalues σ of the matrix of coefficients of this linear set of equations have negative real parts for all values of d, the stationary solutions are stable to infinitesimal perturbations. If any eigenvalue exhibits a positive real part, the solution is unstable. This kind of stability analysis has been carried out for the stationary solutions as a function of α and Ra.

The number of modes for the stability analysis was such that there were no significant differences between the truncation parameters N and $N+2$. In the case of the oscillatory solutions, the comparison with a higher truncation value was possible only up to the Rayleigh number $Ra \sim 700$; above this value we were constrained by the available computer capacity.

Another test of the stability analysis uses the fact that the steady and oscillatory solutions usually exhibit an even parity, i.e. all coefficients with b_{mln} vanish for odd $m+l$. The disturbances of the form (2.3) can thus be separated into those with even and odd parity corresponding to the cases when coefficients $\tilde{b}_{mln}$ with odd $m+l$ or even $m+l$ vanish, respectively. When the truncation N is sufficiently large, even disturbances with $0 \leqslant d \leqslant 0.5$ will give approximately the same growth rate σ as odd disturbances with $0 \leqslant 1-d \leqslant 0.5$.

We have followed the even-roll solution bifurcating at the critical value by increasing the Rayleigh number in small steps. Our results were compared whenever possible with the data as given in the literature by Strauss (1974), Caltagirone (1975), Frick & Müller (1983), Kimura *et al.* (1986) and Steen & Aidun (1988) for the Nusselt

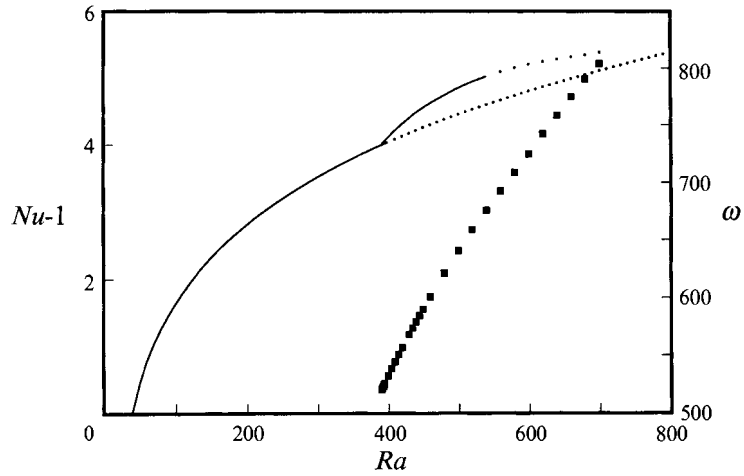

FIGURE 2. Average value of the Nusselt number of the steady and oscillatory solutions as a function of the Rayleigh number for a fixed wavenumber $\alpha = \alpha_c$. The unstable stationary solutions are represented by dots. The frequency of the oscillatory solutions is denoted by squares.

number, the amplitude of the modes or the frequency of the oscillatory solution. Using as initial conditions the values so obtained, we then pursued at each Ra the solutions in α.

3. Steady, spatially periodic solutions

The onset of steady rolls is obtained from the linear stability analysis of the trivial state in equations (2.2*a*) and (2.2*b*). Convection with a given wavenumber sets in when the Rayleigh number exceeds the lowest eigenvalue of the linear problem corresponding to $l = 1, m = 1$, $Ra_0(\alpha) = (\alpha^2 + \pi^2)^2/\alpha^2$. The curve defined by this relationship is the neutral curve. The minimum of the neutral curve is where convection first sets in and is given by the critical Rayleigh number $Ra_c = 4\pi^2$ and wavenumber $\alpha_c = \pi$. A gradual increase of the Rayleigh number will excite only higher modes with $m + l$ =even which describe the even-roll solution.

As the Rayleigh number is increased from the critical value, the higher spatial modes become more and more important (see for instance Strauss 1974). The Nusselt number increases as shown in figure 2. We have plotted the average Nusselt number Nu_0 as a function of the Rayleigh number for the fixed wavenumber $\alpha = \alpha_c$. At the Rayleigh number $Ra = 391 \pm 1$ the steady solution becomes unstable and is replaced by an oscillatory solution with a higher average Nusselt number. This is indicated in figure 2 through the continuation of the steady solution as dotted line and of the oscillatory solution as solid line. The frequency ω of this oscillatory solution is given in the same figure by solid squares. The heat transfer increases more strongly with increasing Rayleigh number after the start of oscillatory convection. The frequency of the oscillatory solutions also increases with the Rayleigh number since it corresponds to the circulation time of convection. Experiments on oscillatory convection made by Koster & Müller (1984) in a Hele-Shaw cell and numerical analysis by Kimura *et al.* 1986 and by Graham & Steen (1994) show a similar behaviour. At $Ra = 545$ this even oscillatory solution becomes unstable and therefore we have replaced the corresponding solid line in figure 2 by a dotted line.

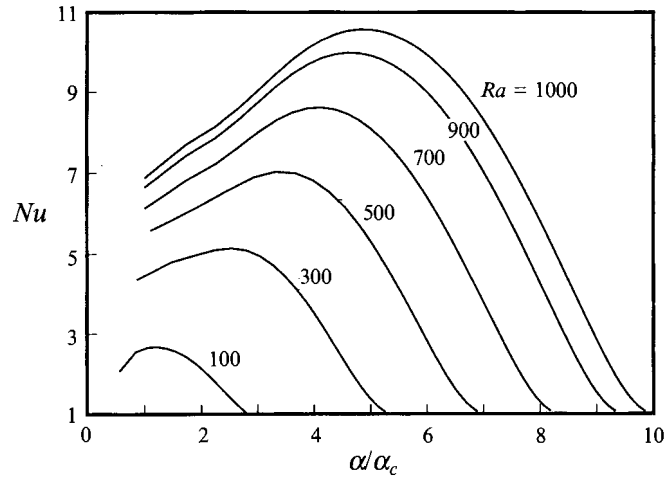

FIGURE 3. Value of the Nusselt number of the steady solutions as a function of the wavenumber α for different values of the Rayleigh number.

For a given Rayleigh number the Nusselt number varies with the wavenumber as shown in figure 3. Evidently the heat transfer is most effective at intermediate wavenumbers between the two extrema determined by the neutral curve. As a consequence, the profile of the horizontally averaged temperature shows a steep variation close to the upper and lower boundaries for the intermediate wavenumbers. The thermal boundary layers become very thin and a higher truncation is needed to study this regime with the same resolution as near the ends of the wavenumber band.

4. Stability of the steady solutions

We have studied the stability of the steady rolls to infinitesimal perturbations of arbitrary wavenumber. This was done, using equations (2.3)–(2.5) without forcing any symmetries on the perturbations, so that modes with amplitudes $\tilde{b}_{mln} \neq \tilde{b}_{m-ln}$ were allowed, as well as modes with any parity in $m + l$.

To study the stability of the stationary solutions in the nonlinear regime, we obtain first their amplitudes via a Newton–Raphson algorithm, as mentioned in §2. With these amplitudes we can calculate the matrix of the coefficients of the set of equations (2.5) in Fourier space. This matrix was diagonalized by reducing it first to a Hessenberg form and then a QR algorithm was used to obtain the eigenvalues (see for instance Press *et al.* 1988).

Similar stability analyses have been carried out for an infinite Hele-Shaw cell by Kvernvold (1979), and for a two-dimensional porous medium by Caltagirone (1975). Caltagirone studied the stability to perturbations with the same wavenumber as the steady solutions and the study was done only up to $Ra = 400$. While our results are generally similar to theirs, there are some differences. This disagreement disappeared when we decreased our truncation parameter N, and considered only perturbations with the same parity as the steady solutions and with $0 \leqslant d \leqslant 0.5$. Under these restrictions we could reproduce quantitatively the stability diagram obtained by Kvernvold, except for a change in the interpretation of two of the stability boundaries:

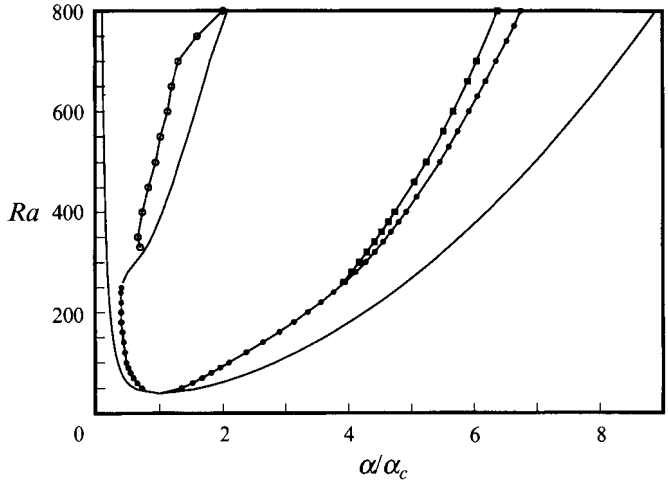

FIGURE 4. Regions of stability of the steady solutions as a function of the Rayleigh number and the wavenumber. The neutral curve is the outer solid line; the Eckhaus instability is plotted as a line with solid circles; the transitions to the different oscillatory instabilities are plotted as a solid line with squares at high wavenumbers and as a solid line at low wavenumbers; the stability limits of the stationary oscillatory solutions are plotted as a solid line with open circles.

the places where the Eckhaus instability and the oscillatory instability occur at low wavenumbers have to be exchanged.

The results of our stability analysis are shown in figure 4. The outer solid line corresponds to the neutral curve where convection sets in. The line with solid circles gives the thresholds for the Eckhaus instability and for a monotonic instability with odd parity. At high wavenumbers there is a line with solid squares that corresponds to an oscillatory growth of the infinitesimal perturbations. At low wavenumbers, the inner solid line corresponds to the transition from steady to oscillatory convection and the solid line with open circles indicates where even oscillatory convection becomes unstable. This figure shows that there is an oscillatory instability predicted for small wavenumbers $\alpha \sim \alpha_c$. This oscillatory state has been observed experimentally by Koster & Müller (1982) and by Daviaud, Bonetti & Dubois (1990), as well as numerically by Frick & Müller (1983) for instance.

A careful study of the stability boundaries to each side of the stable wavenumber band was carried out starting at the critical value Ra_c. Both ends of the stable wavenumber band correspond to an Eckhaus instability up to $Ra_1 = 114 \pm 1$, where we detect for $\alpha = (0.4776 \pm 10^{-4})\alpha_c$ a monotonic instability with maximum growth rate at $d = 0$ which continues along the low-wavenumber end of the stable region. The growth rate of this instability is shown as a function of the perturbation wavenumber d as a solid line with open circles in figure 5 for $Ra = 200$ and $\alpha = 0.4\alpha_c$. When the stability analysis is restricted to even-parity perturbations, this instability grows with $d = 1$, which shows that it is driven by the exponential growth of the odd perturbations. It will be shown in §7 that this instability is related to a spatial 3:1 resonance mechanism.

As the Rayleigh number is increased this situation remains unchanged until we reach $Ra_2 = 218 \pm 1$ and $\alpha = (0.392 \pm 5 \times 10^{-4})\alpha_c$ At this value, an oscillatory instability occurs with $d = 0$ and $\sigma_j \sim 90$ at the low end of the wavenumber band, $\alpha \sim 0.4\alpha_c$. These oscillatory solutions exhibit the same wavelength and parity as the steady rolls

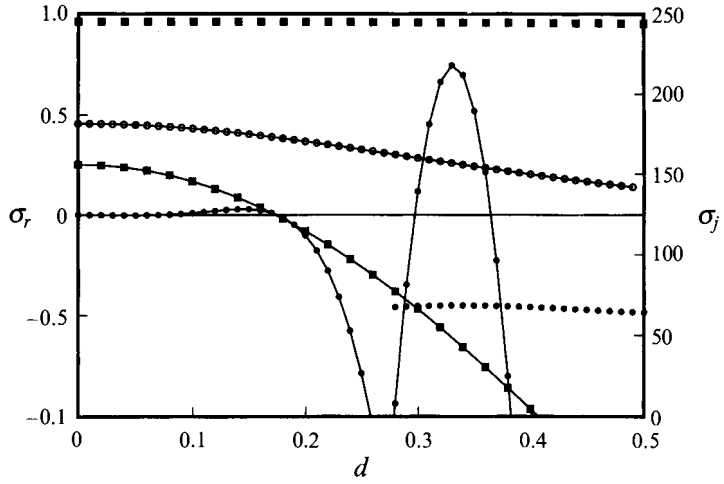

FIGURE 5. Real (solid lines with symbols) and nonzero imaginary parts in j (symbols) of the eigenvalues σ as a function of the perturbation wavenumber d at the point where the steady solutions become unstable: (*a*) open circles for $Ra = 200$, $\alpha/\alpha_c = 0.4$;(*b*) closed circles for $Ra = 255$ $\alpha/\alpha_c = 3.92$; (*c*) solid squares for $Ra = 302$, $\alpha/\alpha_c = 0.8$.

and have been reported in previous work. In figure 5, we have plotted at $Ra = 302$ the real part of the eigenvalues as a solid line with squares and the imaginary part as squares without a line, both as a function of the parameter d.

At $Ra_3 = 251 \pm 1$, $\alpha = (3.865 \pm 10^{-4})\alpha_c$ high-wavenumber rolls become unstable to oscillatory perturbations with a temporal frequency of the order 70 given by the imaginary part of the eigenvalue σ_j, and with a finite wavenumber corresponding to $d = 0.33$. The corresponding growth rates are also shown in figure 5 for $Ra = 255$ and $\alpha = 3.92\alpha_c$ as a line with solid circles for the real part and as solid circles for the imaginary part. Obviously this instability tends to establish a pattern with three times the original wavelength corresponding to rolls with nearly the critical wavelength. This transition and the one due to the odd-mode instability at low α have not been reported in any of the former stability studies where the analysis is restricted to perturbations with even parity and to wavenumbers $0 \leqslant d \leqslant 0.5$. We find under the latter restrictions only an Eckhaus-type or an oscillatory instability on each side of the wavenumber band in agreement with the previous work. We thus conclude that the disturbances admitted by Kvernvold (1979) have not been sufficiently general. The new stability boundary and the Eckhaus stability boundary remain close to each other for Rayleigh numbers up to 800 and beyond as shown in figure 4.

The results obtained for the stability of low-wavenumber rolls are in agreement with the numerical simulations reported in the literature, most of which were done for convection in a square box, where the wavenumber is constrained to be $\alpha = \alpha_c$.

5. Oscillatory solutions

From the results of the stability analysis discussed in §4, we can see that there are two different types of oscillatory instabilities that bifurcate supercritically from the steady solution: At high wavenumbers odd modes grow via a parity-breaking oscillatory bifurcation. This instability evolves into a steady structure with a wavenumber that differs from that of the growing disturbances with odd parity. There will be a short discussion on this instability in §7. The second type of instability has the same

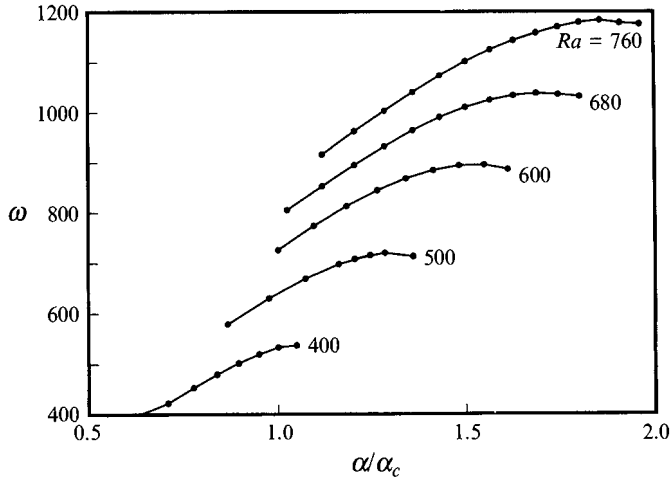

FIGURE 6. Variation of the frequency ω of the stationary oscillatory solutions as a function of the wavenumber for different Rayleigh numbers.

wavelength as the original steady solution, and it is the same as is observed to bifurcate from steady convection in a square box.

When the Rayleigh number is increased smoothly after convection has set in in an infinite layer, the second type of oscillatory convection appears through a supercritical bifurcation from the steady rolls state. This type of even oscillatory convection is stable in the region of parameter space shown in figure 4 between the inner solid line and the line with open circles. We have obtained oscillatory solutions by gradually increasing the Rayleigh number and looking for oscillatory solutions with finite values of the coefficients b_{ml1} at $\alpha \sim \alpha_c$. Once such a solution was obtained, the value of α was changed in small steps. At every step we used the amplitudes obtained with the previous α as initial conditions. In the limit of low wavenumbers, the numerical method did not converge to any stationary oscillatory solution. This problem also occurs in the steady regime. In the case of the steady solutions, this problem is caused by a resonance mechanism (Mizushima & Fujimura 1992). In the resonance mechanism the solution with 3α instead of α tends to be approached. Alternatively a sudden jump into a different type of stationary solution can occur. Nevertheless, the region where even oscillations remain stable is always smaller than the region of α where our algorithm converged to an oscillatory solution, such that this numerical problem did not affect the results of our stability analysis.

As we approach the transition line to the steady solutions, our numerical algorithm always converges. When the maximum values of the b_{ml1} amplitudes are calculated at several values of α approaching the transition, it can be seen that they decay smoothly to zero, while the b_{ml0} amplitudes converge to the ones of the steady solutions. This property is expected since we are dealing with a supercritical bifurcation.

In figure 6 the frequency ω of the solutions has been plotted as a function of the wavenumber at different values of the Rayleigh number. It is seen that, along the transition line between the oscillatory and the steady solutions, the frequency has a finite value different from zero. This value coincides with the values obtained for the imaginary part of the growth rates that are obtained from the stability analysis of the steady state.

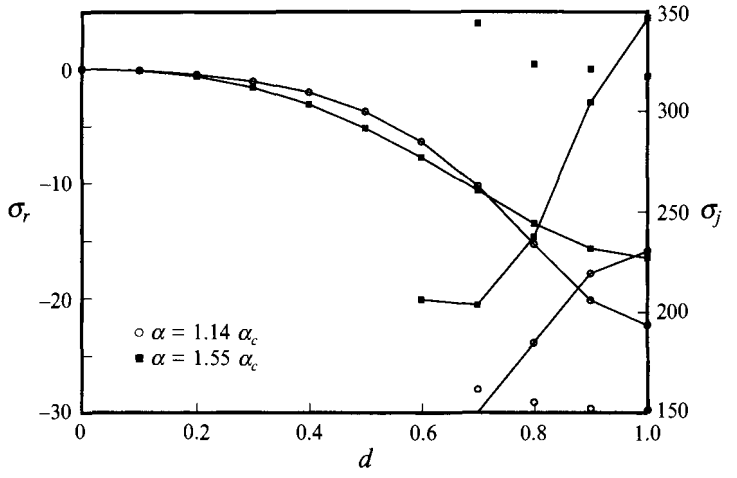

FIGURE 7. Real (solid lines with symbols) and nonzero imaginary (symbols without line) parts of the eigenvalues σ as a function of the Floquet wavenumber d for $Ra = 600$ and α close to the transition into the steady solution (open circles) and close to the transition into unstable even oscillations (solid squares).

6. Stability of the even oscillatory solutions

The transition to complex temporal behaviour in a square cell occurs as a secondary bifurcation of the even oscillatory solutions and its dynamics has therefore been studied via numerical integration by several authors (see for instance Frick & Müller, 1983, Kimura *et al.*, 1986, Caltagirone & Fabrie, 1989). There have been, however, no systematic studies on the stability of the even oscillatory solutions in boxes of infinite horizontal size. The numerical simulations of the transition from the oscillatory state to chaos, although restricted to a fixed geometry, can give some hints about the stability of the time periodic state. Graham & Steen (1992) have studied the different oscillatory solutions that bifurcate from the steady solution, they did not consider perturbations with $d \neq 0$. All authors agree on a scenario for a square box consisting of the transition from steady solutions to oscillatory solutions with a single frequency. At higher values of the control parameter, transitions to a two-frequency quasi-periodic state and further to more complicated states have been obtained.

We have carried out a stability analysis of the even oscillatory solutions based on the numerical technique described in §2. The computer memory requirements for the consideration of perturbations of arbitrary parity could not be satisfied on the available workstations. We thus have restricted ourselves to the study of perturbations with even parity. Since a perturbation of even parity with $d = 0$ corresponds to a perturbation of odd parity with $d = 1$, we have considered the interval of values $0 \leqslant d \leqslant 1$. The only disadvantage of this method of dealing with disturbances of odd parity is a slight degradation in the numerical accuracy. In fact, we tested our method by considering separately perturbations of both even and odd parity, and by checking that they yield the same eigenvalues with a corresponding shift in d.

The analysis was done for several values of the Rayleigh number as a function of the wavenumber α and of the parameter d. In figure 7 a typical result for the stability analysis is shown at a wavenumber close to the transition from oscillatory to steady convection and close to the wavenumber where the oscillatory solution becomes unstable. The real and the nonzero imaginary parts of the eigenvalues with highest growth rates are shown as a function of the perturbation wavenumber d for

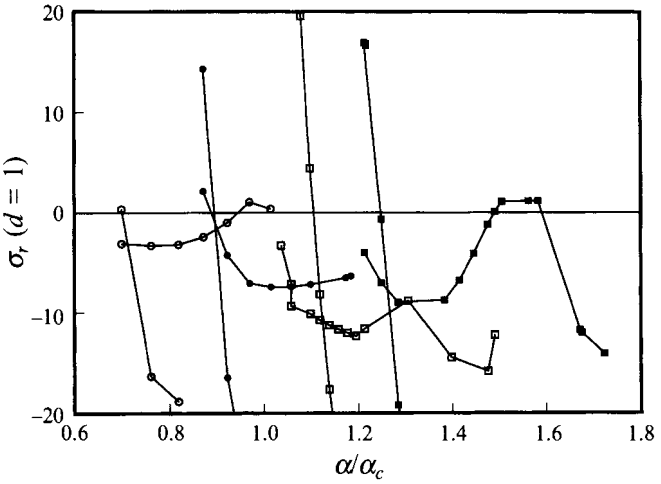

FIGURE 8. Eigenvalues with highest real part for the oscillatory solutions at different values of the Rayleigh number and the wavenumber. Open circles are for $Ra = 400$; solid circles for $Ra = 500$, open squares for $Ra = 600$ and solid squares for $Ra = 700$. For each value of Ra the two perturbations with the largest real part of σ are shown.

$Ra = 600$. At each wavenumber, there are two perturbations that play a dominant role; each of them is characterized by a different imaginary part σ_j. One of the two clearly corresponds to the Eckhaus mode with vanishing imaginary part, but the other does not. Both of them are shown. The highest growth rate corresponds to $d = 0$ as long as α corresponds to a value where even oscillations are stable. But as the wavenumber is decreased, perturbations with $d = 1$ will typically have the highest growth rate. This figure shows that in the low-wavenumber regime, oscillatory solutions lose stability to infinitesimal perturbations of odd parity with a frequency different from that of the stationary oscillatory solutions.

In figure 8 the real part of the eigenvalues σ with perturbation wavenumber $d = 1$ is plotted as a function of the wavenumber α for several values of the Rayleigh number. For each Rayleigh number the two dominant eigenvalues σ are shown. For Rayleigh numbers in the interval $310 \pm 10 < Ra \leqslant 790 \pm 10$ there exists a finite wavenumber band where oscillatory convection is stable with respect to both even and odd perturbations. At $Ra = 700$ there is an interval inside the stable wavenumber band at which the oscillatory solutions become unstable with respect to odd perturbations. At $Ra = 800$ and $Ra = 310$ we have found that even oscillations are unstable within the entire region that could be resolved numerically.

7. Dynamics of disturbances evolving from unstable stationary solutions

In order to check the results of the stability analysis and to understand the dynamics of solutions in the unstable regions, we have carried out direct numerical integrations in time of the solutions in the unstable regions. As initial condition the stationary solution for the given values of the parameters Ra and α was used with slight perturbations added to all coefficients (about 1% of the nearest amplitude value). The Adams–Bashforth scheme has been used for the time integration. The temporal code was implicit in the linear term and explicit for the convolution term. The constant time step was chosen sufficiently small such that the amplitudes obtained

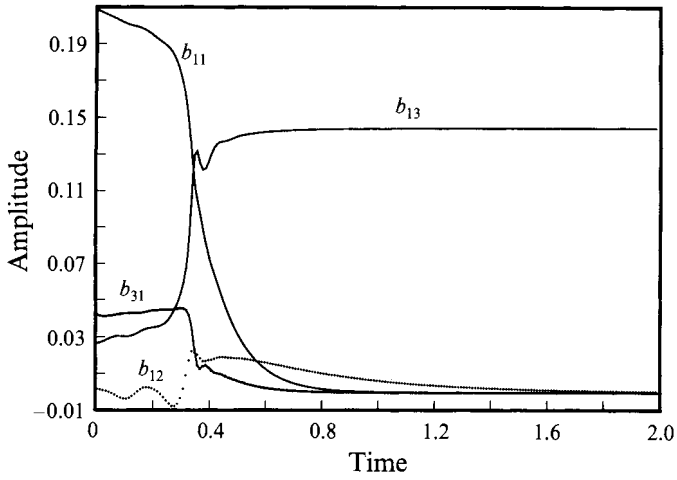

FIGURE 9. Evolution of the even coefficients b_{11}, b_{13}, and b_{31} and the odd coefficient b_{12} as a function of time for $Ra = 200$, $\alpha = 0.39\alpha_c$.

after some transient time did not differ significantly from those obtained with half the time step.

Five cases of special interest have been studied.

The first one corresponds to the sideband instability occurring at $Ra = 200$ and $\alpha = 0.39\alpha_c$. At this value the perturbed steady solution becomes unstable to $d = 0$ perturbations of odd parity. It can be seen in figure 9 that the odd-parity mode b_{12} starts growing exponentially, but, after some transient, decays to zero exponentially. During this time, the b_{11} or b_{31} coefficients have decayed to zero together with the b_{12} coefficient. In their place the b_{13} and b_{33} modes have become dominant. The solution thus has changed into a solution with even parity and three times the initial wavenumber in the horizontal direction. No significant change in the dependence on the vertical coordinate occurs. Accordingly, the new solution lies in the stable region of the wavenumber band.

In the second case $Ra = 300$ and $\alpha = 4.3\alpha_c$ have been used. The time integration was carried out for a longer box fitting 6 convection rolls in the horizontal direction, i.e. we have used periodic conditions with the wavenumber $\alpha/3$. The $b_{1\frac{1}{3}}$ modes correspond to a wavelength which is three times the unit wavelength of the rolls. The time evolution of the $b_{1\frac{1}{3}}$ and the b_{11} modes are shown in figure 10. Instability sets in through a slow oscillatory growth of the $b_{1\frac{1}{3}}$ modes, while the b_{11} modes and the Nusselt number remain almost constant at the beginning. After some time the fundamental mode starts to oscillate and then decays rapidly as the $b_{1\frac{1}{3}}$ mode grows to a value of the same order of magnitude that the fundamental mode had at the beginning of the calculation. This process describes the conversion of the six rolls into two.

A third case was studied at $Ra = 500$ and $\alpha = 0.9\alpha_c$ where the even oscillatory solution becomes unstable to perturbations of higher frequency. After some transient during which odd modes grow, they become periodic in time and add to the even modes. The evolution of the odd and even modes can be seen through the evolution of the b_{11} and b_{12} modes plotted in figure 11(*a*). The corresponding evolution of the Nusselt number has been plotted with a higher resolution at the end of the transient regime in figure 11(*b*). It indicates a superposition of modes with several independent

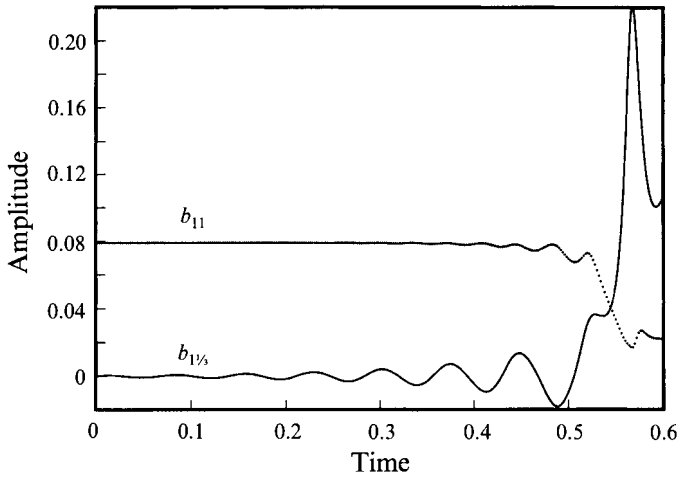

FIGURE 10. Evolution of the long-wavelength coefficient $b_{1\frac{1}{3}}$ and the fundamental coefficient b_{11} as a function of time for $Ra = 300$, $\alpha = 4.3\alpha_c$.

frequencies. The most important ones being $\omega_1 \sim 154$, $\omega_2 \sim 713$ and $\omega_3 \sim 568$. A look at the evolution of the isotherms shown in figure 11(*c*), indicates the breaking of the centrosymmetry of the rolls which is connected with the appearance of odd modes. This situation is different from the one described for the square box by Kimura *et al.* (1986) and confirmed by Caltagirone & Fabrie (1989) in their numerical simulations and by Graham & Steen (1992) in their bifurcation analysis. Kimura *et al.* detected odd oscillations at Rayleigh numbers between 800 and 1000, while before, and below the transition reported in our figure 11, they observe a state which bifurcates from the one-roll solution through a subcritical transition. Our method cannot follow the subcritical branch of a bifurcating solution. Our stability analysis thus seems to have followed at this point a branch of the oscillatory solution which differs from their numerical simulations. Graham & Steen (1994) confirm the coexistence of stable odd- and even-oscillatory solutions above $Ra = 925$, but their non-centrosymmetric branch has not been followed to its point of bifurcation.

The fourth case corresponds to $Ra = 700$ with $\alpha = 1.6\alpha_c$ which falls inside the unstable island. The evolution of the b_{11} and the b_{12} coefficients is shown in figure 12(*a*). The corresponding evolution of the Nusselt number can be seen in figure 12(*b*). After some transient during which the odd modes grow, they decay again and only the even modes persist. This decay could also be due to dissipation in our numerical scheme since the growth rates in this region are not very large. The Nusselt number shows the superposition of the two oscillations driven by the odd and the even modes.

A last case of interest was computed for $Ra = 800$ with the wavenumber $\alpha = 1.92\alpha_c$. These parameter values are very close to the transition from oscillatory to steady behaviour, which occurs at $\alpha = 2.1\alpha_c$. The results are shown in figures 13(*a*) and 13(*b*). In 13(*a*) it is seen that the coefficients with odd $m+l$ start oscillating and seem to dominate the temporal behaviour of the solution. The oscillations of the even coefficient b_{11} seem to follow the perturbation introduced by the oscillatory growth of b_{12}. After some transient time the solution becomes periodic. The Nusselt number shows a period ω of about 1414. But in this case the odd oscillations dominate, so that the mechanism of oscillations differs from the previous cases. The geometry of

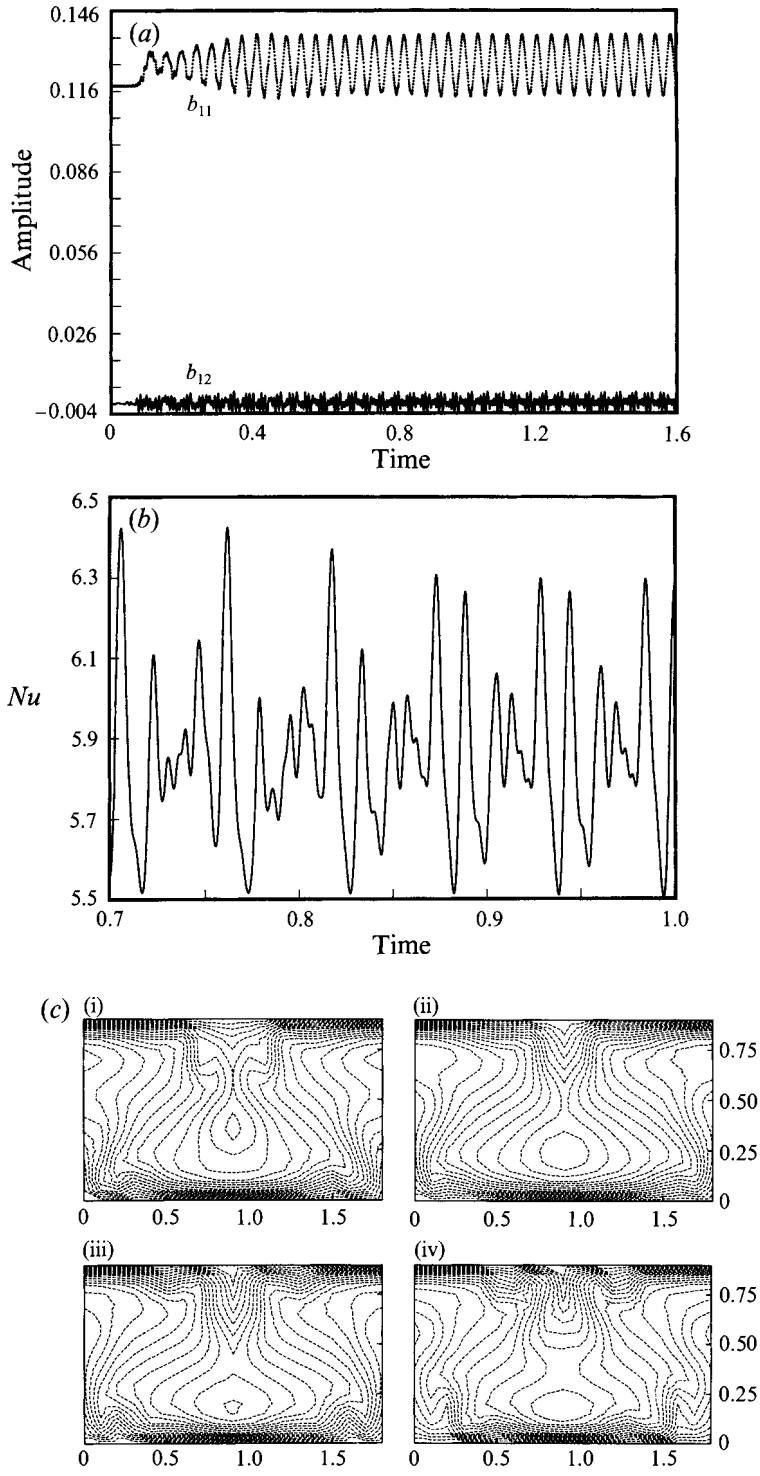

FIGURE 11. (*a*) Evolution of the even coefficient b_{11} and the odd coefficient b_{12} as a function of time for $Ra = 500$, $\alpha = 0.9\alpha_c$. (*b*) Evolution of the Nusselt number for the same values of Ra and α. (*c*) (i)–(iv) isotherms at the times $t = 0.15, t = 0.15108, t = 0.15212, t = 0.15316$ are shown. The corresponding Nusselt numbers are $Nu = 5.87$, 5.57, 5.59, 5.9. Length scales are chosen in units of half the spatial wavelength in each direction.

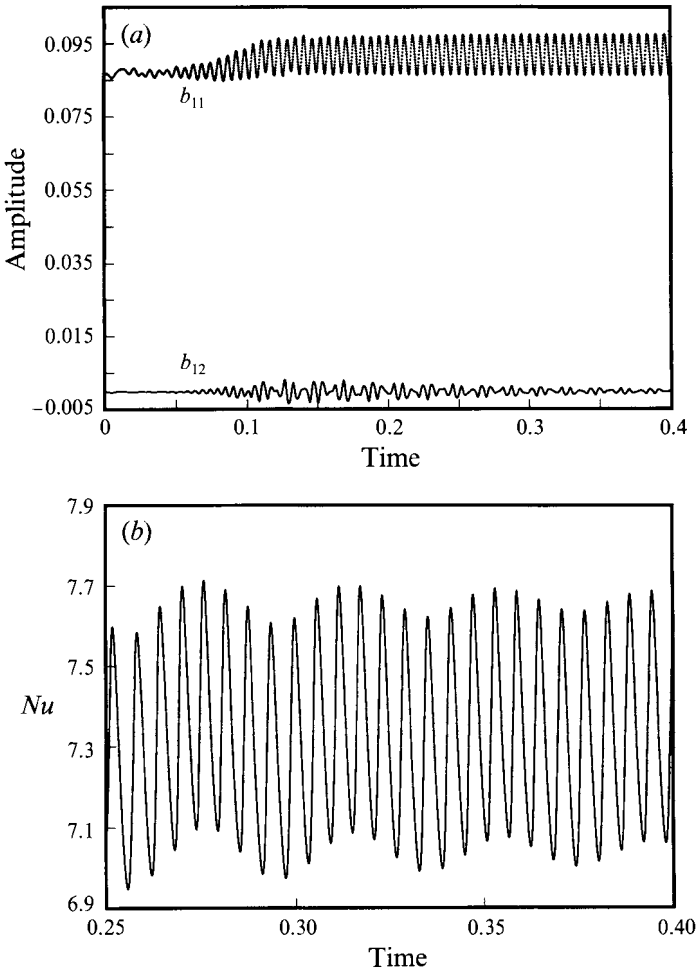

FIGURE 12. (*a*) Evolution of the even coefficient b_{11} and the odd coefficient b_{12} at $Ra = 700$, $\alpha = 1.6\alpha_c$. (*b*) Evolution of the Nusselt number for the same values of Ra and α.

the isotherms as shown in figure 13(*b*) indicates that the oscillations are still due to boundary deformations as in the case with even-parity oscillations, but the rising and falling of the plumes is occurring at a different time, breaking the spatial symmetry of the steady rolls. Since we have not followed systematically the transition line to the instability shown in figure 11, it is not yet clear to us whether both solutions are somehow connected.

8. Summary

We have carried out a detailed stability analysis of two-dimensional steady and oscillatory convection in a porous medium. In particular we have obtained examples of 3:1 resonances akin to those discussed by Mizushima & Fujimura (1992). These resonances are associated with instabilities that have not been reported before and may be related to experimental results observed by Hegseth *et al.* (1992).

The present paper presents a more complete analysis of the instabilities of steady rolls than has been available from previous work. The Eckhaus instability limiting

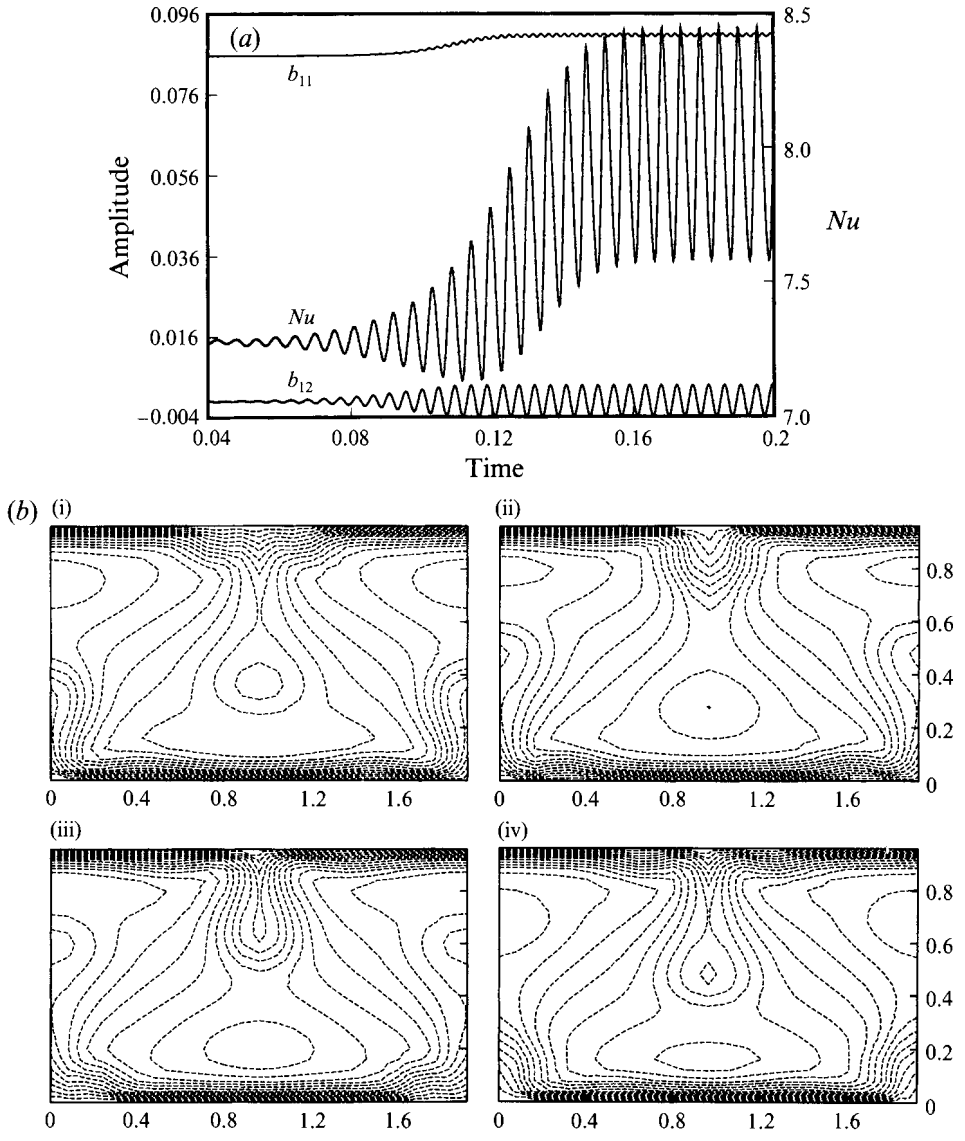

FIGURE 13. (*a*) Evolution of the even coefficient b_{11}, of the odd coefficient b_{12} and of the Nusselt number for $Ra = 800$, $\alpha = 1.92\alpha_c$.(*b*) (i)–(iv) From left to right isotherms at the times $t = 0.15, t = 0.15116, t = 0.1523, t = 0.15344$ are shown. The corresponding Nusselt numbers are $Nu = 8.3$, 7.81, 7.6, 8.29. Length scales are chosen in units of half the spatial wavelength in each direction.

the band of stable wavenumbers at low supercritical Rayleigh numbers is replaced by a sideband instability corresponding to odd-parity perturbations as the Rayleigh number increases. This instability leads to a 3:1 jump in the wavelength. A third instability of oscillatory character occurs at high wavenumbers, which is also related to a 3:1 resonance mechanism and tends to change the wavelength by a finite amount. The fourth instability yields an oscillatory state of even parity for low wavenumbers and for Rayleigh numbers above $Ra = 218$.

In the region where even oscillatory solutions exist, they lose always stability through the growth of odd oscillatory modes. Two cases can be distinguished. In

the first case the odd modes grow while the existing even oscillatory solution persists. Both oscillations coexist and yield a non-centrosymmetric state with several temporal frequencies different from the centrosymmetric one described for the square box by Kimura *et al.* (1986) and confirmed by Caltagirone & Fabrie (1989) in their numerical simulations.

A second transition to non-centrosymmetric convection occurs at Rayleigh numbers above 790: steady convection bifurcates into a regular oscillatory state where the odd modes show large-amplitude oscillations and seem to trigger and dominate the oscillations of the even modes. This type of oscillatory solution for $Ra > 790$ is related to an asymmetry between the rising hot and the falling cold plumes. This differs from the situation reported in earlier works at lower Ra where the lower oscillatory instability keeps the symmetry between both types of plumes.

After the research of this paper had been finished, the authors became aware of the paper by Graham & Steen (1994), which is addressed to the related problem of two-dimensional oscillatory convection in a square box. That article discusses the scaling laws of centrosymmetric solutions above $Ra = 650$ and non-centrosymmetric solutions above $Ra \geqslant 925$. They confirm the results obtained by Kimura *et al.* (1986) and Caltagirone & Fabrie (1989) on this type of oscillation and give a critical value of Ra at which they are stable. These oscillations can be related to those which bifurcate according to our analysis from the steady solution at $Ra = 800$ and $\alpha = 2.1\alpha_c$ or from the centrosymmetric oscillatory solution at $Ra = 500$.

This work was carried out as part of the 'Acción Integrada Hispano-Alemana HA-043 and HA-086'. One of the authors (M.T.J.) is grateful to E. Crespo del Arco for stimulating discussions and to M. Higuera Torrón for her help during the initial stages of this project.

REFERENCES

AHLERS, G. & BEHRINGER, R. P. 1978 Evolution of turbulence from the Rayleigh-Bénard instability. *Phys. Rev. Lett.* **40**, 712–716.

BERGÉ, P. & DUBOIS, M. 1979 Study of unsteady convection through simultaneous velocity and interferometric measurements. *J. Phys. Lett.* **40**, 505.

BUSSE, F. H. 1978 Nonlinear properties of thermal convection. *Rep. Prog. Phys.* **41**, 1929.

CALTAGIRONE, J. P. 1975 Thermoconvective instabilities in a horizontal porous layer. *J. Fluid Mech.* **72**, 269–287.

CALTAGIRONE, J. P. & FABRIE, P. 1989 Natural convection in a porous medium at high Rayleigh numbers. Part I - Darcy's model. *Eur. J. Mech.* B/*Fluids* **8**, 207–227.

DAVIAUD, F., BONETTI, M. & DUBOIS, M. 1990 Transition to turbulence via spatiotemporal intermittency in one-dimensional Rayleigh Bénard convection. *Phys. Rev.* A **42**, 3388–3399.

FRICK, H. & MÜLLER, U. 1983 Oscillatory Hele-Shaw convection. *J. Fluid Mech.* **126**, 521–532.

GOLLUB, J. P. & BENSON, S. V. 1980 Many routes to turbulent convection. *J. Fluid Mech.* **100**, 449–470.

GRAHAM, M. D. & STEEN, P. 1992 Strongly interacting traveling waves and quasiperiodic dynamics in porous medium convection. *Physica* D **54**, 231–350.

GRAHAM, M. D. & STEEN, P. 1994 Plume formation and resonant bifurcations in porous media-convection. *J. Fluid Mech.* **272**, 67–89.

GRAHAM, M. D., MÜLLER, U. & STEEN, P. H. 1992 Time-periodic thermal convection in Hele-Shaw slots: The diagonal oscillation. *Phys. Fluids* A **4**, 2382–2391.

HEGSETH, J., VINCE, J. M., DUBOIS, M. & BERGÉ, P. 1992 Pattern domains in Rayleigh-Bénard slot convection. *Europhys. Lett.* **17**, 413–418.

KIMURA, S., SCHUBERT, G. & STRAUS, J. M. 1986 Route to chaos in porous-medium thermal convection. *J. Fluid Mech.* **166**, 305–324.

KOSTER, J.N. & MÜLLER, U. 1982 Free convection in vertical gaps. *J. Fluid Mech.* **125**, 429–451.

KOSTER, J. N. & MÜLLER, U. 1984 Oscillatory convection in vertical slots. *J. Fluid Mech.* **139**, 363–390.

KRISHNAMURTI, R. 1970*a* On the transition to turbulent convection. Part 1. The transition from two- to three-dimensional flow. *J. Fluid Mech.* **42**, 295–308.

KRISHNAMURTI, R. 1970*b* On the transition to turbulent convection. Part 2. The transition to time dependent flow. *J. Fluid Mech.* **42**, 309–320.

KVERNVOLD, O. 1979 On the stability of non-linear convection in a Hele-Shaw cell. *Intl J. Heat Mass Transfer* **22**, 395-400.

MAURER, J. & LIBCHABER, A. 1979 Rayleigh Bénard experiment in liquid helium: frequency locking and onset of turbulence. *J. Phys. Paris* **40**, 419–423.

MIZUSHIMA, J. & FUJIMURA K. 1992 Higher harmonic resonance of two-dimensional disturbances in Rayleigh-Bénard convection. *J. Fluid Mech.* **234**, 651–667.

PRESS, W. H., FLANNERY, B. P., TEUKOLSKY, S. A. & VETTERLING, W. T. 1988 *Numerical Recipes in C*, pp. 382–394. Cambridge University Press.

RILEY, D. S. & WINTERS, K. H. 1991 Time-periodic convection in porous media: the evolution of Hopf bifurcations with aspect ratio. *J. Fluid Mech.* **223**, 457–474.

STEEN, P. H. & AIDUN, C. K. 1988 Time periodic convection in porous media: transition mechanism. *J. Fluid Mech.* **196**, 263–290.

STRAUSS, J. M. 1974 Large amplitude convection in porous media. *J. Fluid Mech.* **64**, 51–63.

VERONIS, G. 1966 Large-amplitude Bénard convection *J. Fluid Mech.* **26** 49–68.

WOODING, R. A. 1960, Instability of a viscous liquid of variable density in a vertical Hele-Shaw cell. *J. Fluid Mech.* **7**, 501–515.